Hindawi
International Journal of Aerospace Engineering
Volume 2024, Article ID 2541698, 15 pages
https://doi.org/10.1155/2024/2541698

Research Article

VGESO-Based Finite-Time Fault-Tolerant Tracking Control for Quadrotor Unmanned Aerial Vehicle

Haidong Shen,[1] **Jiwei Du**,[2] **Kun Yan**,[2] **Yanbin Liu**,[1] **and Jinbao Chen**[1]

[1]*College of Astronautics, Nanjing University of Aeronautics and Astronautics, Nanjing 211106, China*
[2]*School of Electronic Information Engineering, Xi'an Technological University, Xi'an 710021, China*

Correspondence should be addressed to Haidong Shen; shenhaidong@nuaa.edu.cn

Received 31 October 2023; Revised 6 January 2024; Accepted 18 January 2024; Published 2 February 2024

Academic Editor: Binbin Yan

Based on the variable gain extended state observer, a finite-time fault-tolerant control strategy is developed for the quadrotor unmanned aerial vehicle with actuator faults and external disturbances. Firstly, a novel variable gain extended state observer is designed to estimate the unknown external disturbances, which mitigates the initial peaking phenomenon existing in traditional extended state observer-based methods. Meanwhile, the neural networks are applied to accurately approximate unknown couplings online. Moreover, with the help of the projection operator technique, the unknown actuator faults are observed in real time. Combined with the backstepping framework, the finite-time robust fault-tolerant control scheme is constructed and the stability is strictly proved via Lyapunov's theory. Finally, the validity of the developed control scheme is demonstrated through numerical simulations.

1. Introduction

With the reformation and development of automatic control theory, the quadrotor unmanned aerial vehicle (UAV) has attracted wide attention in different fields. Owing to the advantages of low-speed flight, low-altitude hovering, vertical takeoff, and landing, it can not only be applied to many civilian areas but also has pivotal practical utility in the military and national defense fields [1, 2]. However, the quadrotor UAV is not only a typical underactuated system but also impressionable to the actuator faults and external disturbances because of the unique rotor structures [3]. Therefore, high-efficiency robust fault-tolerant control (FTC) design for the quadrotor UAV is a challenging topic worthy of intensive study.

Disturbances exist in almost all industrial systems and adversely affect control performance. Consequently, various antidisturbance methods have been presented to assure the system tracking performance in recent years, such as robust control [4, 5], sliding mode control [6–9], disturbance observer-based control [10, 11], and active disturbance rejection control (ADRC) [12–16]. Sliding mode control is widely used due to its robustness and fast response. Among these methods, the ADRC technique has been extensively used because of its ability to estimate total unknown uncertainties and disturbances [12]. As an important part of the ADRC technique, the high-quality extended state observer (ESO) can enhance the robustness of the system. In [13], a high-order ESO-based trajectory tracking control method was proposed for the quadrotor UAV in the presence of position constraints and uncertainties. In [14], an ESO-based robust deadbeat current controller was developed for the permanent magnet synchronous machine system with mismatch parameters and unmodeled nonlinear elements. In [15], the sliding mode approach was combined with the ESO approach to stabilize the pneumatic servo system subject to unknown disturbances. In [16], a deep forest algorithm-based fault diagnosis and location algorithm was presented for the quadrotor UAV system by means of the ESO technique. Nevertheless, most of the existing research results related to the ADRC methods were based on the constant observation gain, which always requires large values to

ensure the rapid convergence of observation errors. For this reason, there is a so-called initial peaking phenomenon in the early operation of the observer existing in the traditional ESO method, and it is unfavorable to the transient dynamic response of the system. Therefore, novel variable gain extended state observer (VGESO) needs further exploration to enhance the antidisturbance performance.

Furthermore, actuator fault is another important factor that threatens the safe flight of quadrotor UAV. If the actuator fault cannot be handled in a timely manner, it will not only affect the flight control performance but also cause property losses in serious cases. At present, the adaptive estimation scheme is widely adopted to deal with the unknown fault due to its direct observation capability. In [17], an adaptive FTC strategy was developed for quadrotor UAV systems under actuator faults. In [18], an output feedback-based robust adaptive fault estimation strategy was presented for the quadrotor attitude system with actuator faults. In [19], sensor faults were studied for the switched uncertain nonlinear systems based on fuzzy control technology. In [20], a distributed fault estimation method was presented for the heterogeneous multiagent systems. Radial basis function neural networks (RBFNNs) are commonly utilized to approach continuous unknown functions. In [21], a neural FTC strategy was developed to address uncertainties existing in the helicopter system. In [22], a fuzzy neural network PID control method was presented to restrain the adverse impact of actuator faults. However, most of the existing works focus on the asymptotic stability of the quadrotor UAV under actuator faults, and the finite-time stability needs further consideration.

Since the operational missions of the quadrotor UAV become more and more complicated, it is of practical significance to address the finite-time convergence problem. In [8], the problem of finite-time stability was discussed for the variable sweep morphing aircraft based on the adaptive supertwisting sliding mode control method. In [23], a finite-time terminal sliding mode control scheme was developed for UAV systems with load suspension. In [24], a backstepping-based finite-time controller was presented for the disturbed quadrotor UAV system. Considering the dynamic obstacle disturbances, a finite-time controller was developed for the quadrotor UAV system in [25]. In [26], the issue of time-triggered-based finite-time control was investigated for the quadrotor system. In [27], an adaptive sliding mode finite-time stabilization control method was designed for the UAV system with parametric uncertainties. However, reviewing the reported literature, the high-quality finite-time FTC design for quadrotor UAV subject to external disturbance and actuator fault deserves more attention.

In general, a VGESO-based finite-time FTC algorithm is developed for the quadrotor UAV to guarantee flight safety and mission success. The main contributions of this work are summarized as follows:

(1) A novel VGESO is developed to deal with the unknown disturbance, which can overcome the initial peaking phenomenon existing in the traditional ESO approach

(2) The adaptive fault observer is combined with the RBFNN technique to estimate the unknown actuator fault directly

(3) The presented antidisturbance FTC strategy can make the quadrotor UAV accomplish the tracking mission in finite time

The rest of this article is organized as follows. In Section 2, the nonlinear dynamic equations of the quadrotor UAV are established and some necessary assumptions are given. In Section 3, the robust fault-tolerant controller design and stability analysis are introduced. In Section 4, contrastive numerical simulations are conducted to demonstrate the effectiveness of the developed technique. In Section 5, conclusions and prospects are given.

2. Problem Description

The schematic diagram of the quadrotor UAV is given in Figure 1, where $R_e = \{o_e, x_e, y_e, z_e\}$ defines the earth frame fixed on a point on Earth and $R_b = \{o_b, x_b, y_b, z_b\}$ denotes the body coordinate frame fixed on the centroid of the quadrotor UAV. Then, taking both actuator faults and external disturbances into account, the complete dynamic equations of quadrotor UAVs are derived based on Newton-Euler theory as follows [28]:

$$\begin{aligned}
\ddot{x} &= \frac{\rho_1 u_1}{m}(\cos\phi\sin\theta\cos\psi + \sin\phi\sin\psi) + d_{11},\\
\ddot{y} &= \frac{\rho_1 u_1}{m}(\cos\phi\sin\theta\sin\psi - \cos\psi\sin\phi) + d_{12},\\
\ddot{z} &= \frac{\rho_1 u_1}{m}\cos\theta\cos\phi - g + d_{13},\\
\dot{\phi} &= \varsigma + \upsilon\sin\phi\tan\theta + \mu\tan\theta\cos\phi,\\
\dot{\theta} &= -\mu\sin\phi + \upsilon\cos\phi,\\
\dot{\psi} &= \frac{\mu\cos\phi}{\cos\theta} + \frac{\upsilon\sin\phi}{\cos\theta},\\
\dot{\varsigma} &= \upsilon\mu\left(\frac{J_y - J_z}{J_x}\right) + \frac{\rho_{21}u_2}{J_x} + d_{21},\\
\dot{\upsilon} &= \varsigma\mu\left(\frac{J_z - J_x}{J_y}\right) + \frac{\rho_{22}u_3}{J_y} + d_{22},\\
\dot{\mu} &= \varsigma\upsilon\left(\frac{J_x - J_y}{J_z}\right) + \frac{\rho_{23}u_4}{J_z} + d_{23},
\end{aligned} \tag{1}$$

where $\Upsilon = [x, y, z]^T$ denotes the position vector defined in R_e; $\Lambda = [\phi, \theta, \psi]^T$ represents the attitude angle including roll angle ϕ, pitch angle θ, and yaw angle ψ; $\Theta = [\varsigma, \upsilon, \mu]^T$ is the angular rate defined in R_b; u_1 is the total thrust; $M = [u_2, u_3, u_4]^T$ is the control moment; m is the mass; g is the acceleration of gravity; $J = \mathrm{diag}\{J_x, J_y, J_z\}$ is the moment of inertia matrix; ρ_1 and $\rho_{2i}(i = 1, 2, 3)$ define the constant partial loss of effectiveness (LOE) fault factor of corresponding

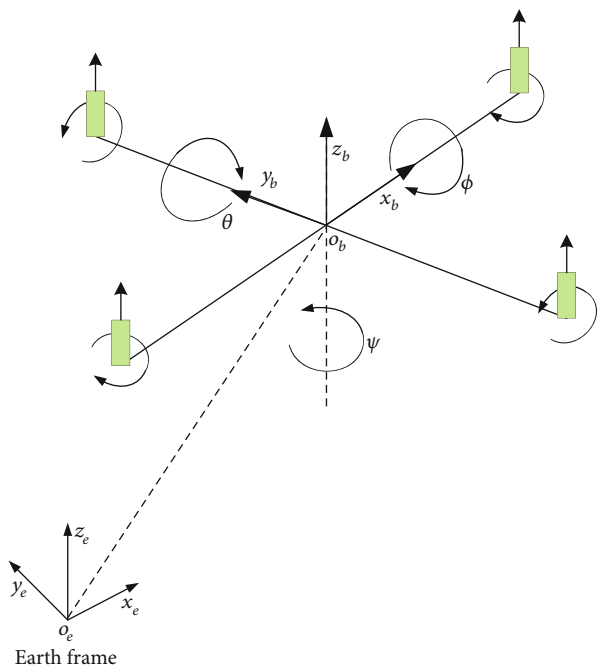

Figure 1: Coordinate system of the quadrotor UAV.

actuator; and $d_j = [d_{j1}, d_{j2}, d_{j3}]^T (j = 1, 2)$ represents unknown external disturbances.

The primary control objective of this study is to develop an effective robust fault-tolerant controller, which simultaneously guarantees that

(1) all errors of the closed-loop system are bounded

(2) the desired trajectories can be tracked in finite time

Meanwhile, the following assumptions and lemmas are given.

Assumption 1 (see [29]). The external disturbances are assumed to be bounded satisfying $\|d_1\| \le R_1$, $\|\dot{d}_1\| \le R_2$, $\|d_2\| \le R_3$, and $\|\dot{d}_2\| \le R_4$, where R_1, R_2, R_3, and R_4 are positive constants. Moreover, the actuator LOE fault factors ρ_1 and ρ_{2i} are assumed to be constant and belong to $[\varepsilon, 1]$, where $\varepsilon > 0$ is the lower bound.

Lemma 2 (see [21]). *RBFNNs are commonly used for approximate unknown continuous functions $f(F_m)$: $R^n \longrightarrow R$, which can be written in the form of*

$$f(F_m) = \widehat{W}^T h(F_m) + \wp, \tag{2}$$

where $F_m \in R^n$ is the input variable vector and $\wp$ is the resulting approximation error, $\widehat{W} \in R^j$ stands for the estimation of the optimum weight vector W^*, and $h(F_m) = [h_1(F_m), h_2(F_m), \cdots, h_j(F_m)] \in R^j$ represents the basis function. The optimal weight vector of the RBFNN is defined as

$$W^* = \arg \min_{\widehat{W} \in \Omega_f} \left[\sup_{F_m \in \Omega_{F_m}} \left| \widehat{f}(F_m | \widehat{W}) - f(F_m) \right| \right], \tag{3}$$

where $\Omega_f = \{\widehat{W} : \|\widehat{W}\| \le \bar{W}\}$ is a valid set with $\bar{W}$ being a constant and Ω_M is an acceptable set of the state. Substituting the optimal weight value results in

$$f(F_m) = W^{*T} h(F_m) + \wp^*, \tag{4}$$

where $\wp^*$ is the optimal approximation error satisfying $|\wp^*| \le \bar{\wp}$ with $\bar{\wp}$ being a constant.

Lemma 3 (see [30]). *For any real numbers $b_i (i = 1, 2, \cdots, n)$, the following inequalities hold:*

$$\begin{aligned} \left(\sum_{i=1}^{n} |b_i| \right)^{\sigma} &\le \sum_{i=1}^{n} |b_i|^{\sigma}, \\ \left(\sum_{i=1}^{n} |b_i|^2 \right)^{\iota} &\le \left(\sum_{i=1}^{n} |b_i|^{\iota} \right)^2, \end{aligned} \tag{5}$$

where $0 < \sigma < 1$ and $0 < \iota < 2$.

Lemma 4 (see [30]). *For arbitrary positive constants ϖ_1, ϖ_2, and ϖ_3, the following inequation holds:*

$$|\kappa_1|^{\varpi_1} |\kappa_2|^{\varpi_2} \le \frac{\varpi_1}{\varpi_1 + \varpi_2} \varpi_3 |\kappa_1|^{\varpi_1 + \varpi_2} + \frac{\varpi_2}{\varpi_1 + \varpi_2} \varpi_3^{\varpi_1/\varpi_2} |\kappa_2|^{\varpi_1 + \varpi_2}, \tag{6}$$

where κ_1 and κ_2 are real values.

Lemma 5 (see [30, 31]). *For the given nonlinear system, if there exists a smooth positive definite function $V(x)$ satisfying $\dot{V}(x) \le -\tau_1 V^{\eta}(x) + \tau_2$, where real numbers satisfy $\tau_1 > 0$, $0 < \eta < 1$, and $0 < \tau_2 < \infty$, the system states convergence in finite time, with the settling time T_{st} defined as $T_{st} \le (1/(1-\eta) K_d \tau_1)[V_3^{1-\eta}(0) - (\tau_2/((1-K_d)\tau_1))^{(1-\eta)/\eta}]$, where $0 < K_d < 1$ is a constant.*

3. Finite-Time Fault-Tolerant Controller Design

In this section, the design process of the proposed finite-time robust fault-tolerant controller is introduced elaborately, with the flow chart presented in Figure 2.

3.1. VGESO Design of Position Loop. For the sake of clarity, we rewrite the position loop governing equations of quadrotor UAV as

$$\begin{aligned} \dot{\Upsilon} &= \Delta, \\ \dot{\Delta} &= \rho_1 B U - g\vartheta + d_1, \end{aligned} \tag{7}$$

where Δ is the velocity vector, $B = \text{diag}\{u_x/m, u_y/m, u_z/m\}$, $u_x = \sin\psi \sin\phi + \cos\psi \cos\phi \sin\theta$, $u_y = \sin\psi \cos\phi \sin\theta -$

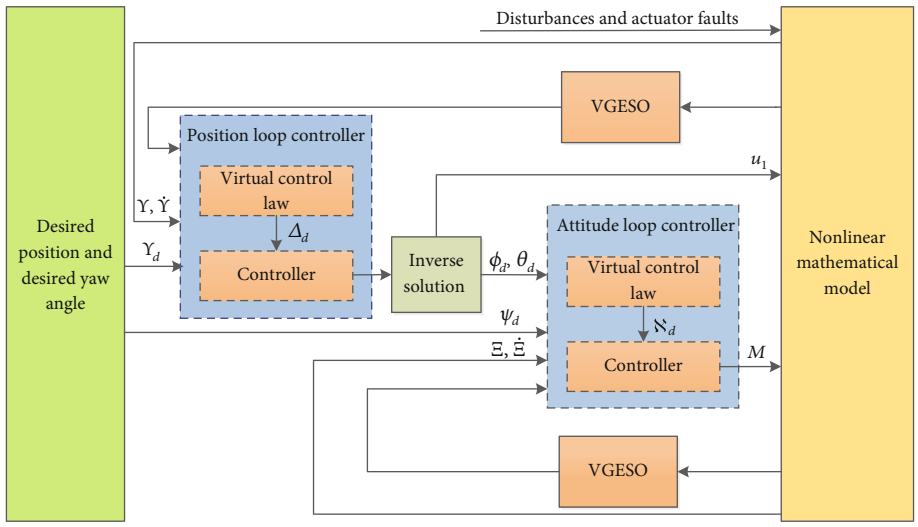

Figure 2: Block diagram of controller design.

$\cos\psi \sin\phi$, $u_z = \cos\theta\cos\phi$, $U = [u_1, u_1, u_1]^T$, and $\vartheta = [0, 0, 1]^T$.

Based on Lemma 2, the following approximation of the unknown coupling term $\rho_1 BU$ can be obtained:

$$L_1 \rho_1 BU = W_1^{*T} h(BU) + \wp_1^*, \tag{8}$$

where $L_1 \in R^{3\times3}$ defines the positive diagonal matrix, $W_1^* \in R^{j\times3}$ is the optimal weight matrix satisfying $\|W_1^*\| \le \bar{W}_1$, $h(BU) \in R^{j\times1}$ is the Gaussian basis function vector and $\|h(BU)\| \le \delta_1$, and $\wp_1^*$ is the approximate error.

Define $\Delta = x_1$ and $d_1 = x_2$. Then, we have

$$\begin{aligned} \dot{x}_1 &= L_1^{-1} W_1^{*T} h(BU) + L_1^{-1}\wp_1^* - g\vartheta + x_2, \\ \dot{x}_2 &= \dot{d}_1. \end{aligned} \tag{9}$$

According to (9), the VGESO is expressed as

$$\begin{aligned} \dot{\hat{x}}_1 &= -\beta_1(t) z_1 + L_1^{-1} \hat{W}_1^T h(BU) - g\vartheta + \hat{x}_2, \\ \dot{\hat{x}}_2 &= -\beta_2(t) z_1, \end{aligned} \tag{10}$$

where $\hat{x}_i (i = 1, 2)$ represents the estimation of x_i; $z_1 = \hat{x}_1 - x_1$;

$$Y_1(t) = \begin{cases} \gamma_1 / \|z_1\|^2, & \|z_1\| \ge h_1, \\ \gamma_2, & \text{other}; \end{cases} \tag{11}$$

$\beta_1(t) = \operatorname{diag}\{Y_1(t)/2, Y_1(t)/2, Y_1(t)/2\}$; $\beta_2(t) = \operatorname{diag}\{Y_1(t), Y_1(t), Y_1(t)\}$; γ_1, h_1, and γ_2 are positive constants; and $\hat{W}_1$ is the estimation of W_1.

Considering (9) and (10), the observation errors of the VGESO can be expressed as

$$\begin{aligned} \dot{z}_1 &= -\beta_1(t) z_1 + L_1^{-1} \tilde{W}_1^T h(BU) - L_1^{-1}\wp_1^* + z_2, \\ \dot{z}_2 &= -\beta_2(t) z_1 - \dot{d}_1, \end{aligned} \tag{12}$$

where $z_2 = \hat{x}_2 - x_2$ and $\tilde{W}_1 = \hat{W}_1 - W_1^*$.

Define $\Sigma_1 = [z_1, z_2]^T$. Then, we can obtain

$$\begin{aligned} \dot{\Sigma}_1 = \begin{bmatrix} \dot{z}_1 \\ \dot{z}_2 \end{bmatrix} &= \begin{bmatrix} -\beta_1(t) & 1 \\ -\beta_2(t) & 0 \end{bmatrix} \Sigma_1 + \begin{bmatrix} L_1^{-1} \tilde{W}_1^{*T} h(BU) \\ 0 \end{bmatrix} \\ &+ \begin{bmatrix} -L_1^{-1}\wp_1^* \\ -\dot{d}_1 \end{bmatrix} = A_1 \Sigma_1 + B_1 + B_2. \end{aligned} \tag{13}$$

For the purpose of ensuring A_1 is Hurwitz matrix, the parameters satisfy $\beta_1(t) > 0$ and $\beta_2(t) > 0$. To put it differently, there is a positive definite matrix

$$P_1 = \begin{bmatrix} P_{11} & P_{12} \\ P_{13} & P_{14} \end{bmatrix}, \tag{14}$$

which satisfies

$$A_1{}^T P_1 + P_1 A_1 = -Q_1, \tag{15}$$

where Q_1 represents the positive definite matrix.

Remark 6. In the initial phase of ESO estimation, owing to the large initial error between the estimated signal and actual value, a large overshoot will appear in the early adjustment process. This is the so-called initial peaking phenomenon [32, 33]. The VGESO designed above can solve the initial peaking problem by using a small gain at first and then

maintaining a high gain, which upgrades the practical application and ensures observation accuracy.

3.2. Robust Fault-Tolerant Controller Design of Position Motion. Tracking errors of position motion are defined as

$$e_1 = \Upsilon_d - \Upsilon, \tag{16}$$

$$e_2 = \Delta_d - \Delta, \tag{17}$$

where $\Upsilon_d = [x_d, y_d, z_d]^T$ denotes the desired position and $\Delta_d = [u_d, v_d, w_d]^T$ is the virtual controller.

Combining (7) and (17), the derivative of (16) is

$$\dot{e}_1 = \dot{\Upsilon}_d - \Delta_d + e_2. \tag{18}$$

The virtual controller Δ_d is designed as

$$\Delta_d = \dot{\Upsilon}_d + k_1 e_1^{2\pi_1 - 1}, \tag{19}$$

where $k_1 = \mathrm{diag}\,\{k_{11}, k_{12}, k_{13}\} > 0$ and $0.5 < \pi_1 < 1$.

Considering (19), equation (18) can be further described as

$$\dot{e}_1 = -k_1 e_1^{2\pi_1 - 1} + e_2. \tag{20}$$

Then, differentiating (17) yields

$$\dot{e}_2 = \dot{\Delta}_d - \rho_1 BU + g\vartheta - d_1. \tag{21}$$

The position loop finite-time controller is proposed as

$$BU = \frac{1}{\rho_1}\left(\dot{\Delta}_d + g\vartheta - d_1 + k_2 e_2^{2\pi_1 - 1} + e_1 + s_1 e_2\right), \tag{22}$$

where s_1 is the proposed positive definite matrix.

Define $a_1 = 1/\rho_1$. Since $\rho_1 \in [\varepsilon, 1]$, it can be seen that $a_1 \in [1, 1/\varepsilon]$. Then, (22) becomes

$$BU = \hat{a}_1\left(\dot{\Delta}_d + g\vartheta - \hat{x}_2 + k_2 e_2^{2\pi_1 - 1} + e_1 + s_1 e_2\right), \tag{23}$$

where $\hat{a}_1$ is the estimate of a_1.

Combining (23), equation (21) can be expressed as

$$\begin{aligned}\dot{e}_2 &= \dot{\Delta}_d - \frac{\hat{a}_1}{a_1}\left(\dot{\Delta}_d + g\vartheta - \hat{x}_2 + k_2 e_2^{2\pi_1 - 1} + e_1 + s_1 e_2\right)\\ &\quad + g\vartheta - d_1 = -e_1 - k_2 e_2^{2\pi_1 - 1} + z_2 - s_1 e_2\\ &\quad - \frac{\tilde{a}_1}{a_1}\left(\dot{\Delta}_d + g\vartheta - \hat{x}_2 + k_2 e_2^{2\pi_1 - 1} + e_1 + s_1 e_2\right),\end{aligned} \tag{24}$$

where $\tilde{a}_1 = \hat{a}_1 - a_1$.

Select the Lyapunov candidate function as

$$\begin{aligned}V_1 &= \frac{1}{2} a_1 {e_1}^T e_1 + \frac{1}{2} a_1 {e_2}^T e_2 + \frac{1}{2r_1} {\tilde{a}_1}^2\\ &\quad + \frac{1}{2} tr\left\{\tilde{W}_1^T T_1^{-1} \tilde{W}_1\right\} + \Sigma_1^T P_1 \Sigma_1,\end{aligned} \tag{25}$$

where $r_1 > 0$ and $T_1 = T_1^T > 0$ are the appropriate parameters.

Considering (20) and (24), the derivative of (25) is given by

$$\begin{aligned}\dot{V}_1 &= a_1 e_1^T\left(-k_1 e_1^{2\pi_1 - 1} + e_2\right) + a_1 e_2^T\Big(-e_1 - k_2 e_2^{2\pi_1 - 1} + z_2 - s_1 e_2\\ &\quad - \frac{\tilde{a}_1}{a_1}\left(\dot{\Delta}_d + g\vartheta - \hat{x}_2 + k_2 e_2^{2\pi_1 - 1} + e_1 + s_1 e_2\right)\Big)\\ &\quad + \frac{1}{r_1}\tilde{a}_1 \dot{\hat{a}}_1 + tr\left\{\tilde{W}_1^T T_1^{-1} \dot{\hat{W}}_1\right\} + \Sigma_1^T P_1 \dot{\Sigma}_1 + \dot{\Sigma}_1^T P_1 \Sigma_1\\ &\le -a_1 e_1^T k_1 e_1^{2\pi_1 - 1} - a_1 e_2^T k_2 e_2^{2\pi_1 - 1} + a_1 e_2^T z_2 - a_1 e_2^T s_1 e_2\\ &\quad - e_2^T \tilde{a}_1 \Gamma_1 + \frac{1}{r_1}\tilde{a}_1 \dot{\hat{a}}_1 + tr\left\{\tilde{W}_1^T T_1^{-1} \dot{\hat{W}}_1\right\} - \Sigma_1^T Q_1 \Sigma_1\\ &\quad + 2\Sigma_1^T P_1 B_1 + 2\Sigma_1^T P_1 B_2,\end{aligned} \tag{26}$$

where $\Gamma_1 = \dot{\Delta}_d + g\vartheta - \hat{x}_2 + k_2 e_2^{2\pi_1 - 1} + e_1 + s_1 e_2$.

The parameter update law and adaptive fault observer are designed as

$$\begin{aligned}\dot{\hat{W}}_1 &= -T_1\left(2h(BU) z_1^T P_{11} L_1^{-1} + G_{n1}\hat{W}_1\right),\\ \dot{\hat{a}}_1 &= \mathrm{Proj}_{[1,1/\varepsilon]}\left\{r_1 {\Gamma_1}^T e_2\right\} - r_1 G_{m1}\hat{a}_1,\end{aligned} \tag{27}$$

where G_{n1} and G_{m1} are designed positive constants, $\mathrm{Proj}\{\cdot\}$ is the projection operator, and its role is to project $\hat{a}_1$ into $[1, 1/\varepsilon]$ [34].

Defining $N_1 = (1/r_1)\tilde{a}_1 \dot{\hat{a}}_1$, $N_2 = tr\{\tilde{W}_1^T T_1^{-1} \dot{\hat{W}}_1\}$, and $N_3 = -\Sigma_1^T Q_1 \Sigma_1 + 2\Sigma_1^T P_1 B_1 + 2\Sigma_1^T P_1 B_2$, we can get

$$\begin{aligned}N_1 &= \Gamma_1^T e_2 \tilde{a}_1 - G_{m1}\tilde{a}_1 a_1 - G_{m1}{\tilde{a}_1}^2\\ &\le \Gamma_1^T e_2 \tilde{a}_1 - \frac{1}{2} G_{m1}{\tilde{a}_1}^2 + \frac{1}{2\varepsilon^2} G_{m1},\end{aligned} \tag{28}$$

$$\begin{aligned}N_2 &= -2tr\left\{\tilde{W}_1^T h(BU) z_1^T P_{11} L_1^{-1}\right\} - G_{n1} tr\left\{\tilde{W}_1^T\left(\tilde{W}_1 + W_1^*\right)\right\}\\ &\le -2tr\left\{\tilde{W}_1^T h(BU) z_1^T P_{11} L_1^{-1}\right\} - G_{n1}\left\|\tilde{W}_1^T\right\|^2 + \frac{1}{2} G_{n1}\left\|\tilde{W}_1\right\|^2\\ &\quad + \frac{1}{2} G_{n1}\left\|W_1^*\right\|^2 \le -2tr\left\{\tilde{W}_1^T h(BU) z_1^T P_{11} L_1^{-1}\right\}\\ &\quad - \frac{1}{2} G_{n1}\left\|\tilde{W}_1\right\|^2 + \frac{1}{2} G_{n1}\bar{W}_1^2,\end{aligned} \tag{29}$$

$$\begin{aligned} N_3 &\le -\Sigma_1^T Q_1 \Sigma_1 + 2\left\|\Sigma_1^T\right\|\|P_1\|\|B_2\| + 2z_1^T P_{11} L_1^{-1} \tilde{W}_1^T h(BU) \\ &\quad + 2z_2^T P_{13} L_1^{-1} \tilde{W}_1^{*T} h(BU) \le -\Sigma_1^T (Q_1 - \lambda_1 I)\Sigma_1 + \frac{C_1^2}{\lambda_1} \\ &\quad + 2z_1^T P_{11} L^{-1} \tilde{W}_1^T h(BU) + \lambda_2 C_2^2 z_2^T z_2 + \frac{\left\|\tilde{W}_1^T\right\|^2}{\lambda_2}, \end{aligned} \tag{30}$$

where λ_1 and λ_2 are designed positive parameters, $\|P_1\|\|B_2\| \le C_1$, and $\|P_{13}\|\|L_1^{-1}\|\|h(BU)\| \le C_2$.

Substituting (28), (29), and (30) into (26), we have

$$\begin{aligned} \dot{V}_1 &\le -a_1 e_1^T k_1 e_1^{2\pi_1 - 1} - a_1 e_2^T k_2 e_2^{2\pi_1 - 1} + a_1 e_2^T z_2 - a_1 e_2^T s_1 e_2 \\ &\quad - \frac{1}{2} G_{m1} \tilde{a}_1{}^2 + \frac{1}{2\varepsilon^2} G_{m1} - \frac{1}{2} G_{n1} \left\|\tilde{W}_1\right\|^2 + \frac{1}{2} G_{n1} \bar{W}_1^2 \\ &\quad - \Sigma_1^T (Q_1 - \lambda_1 I)\Sigma_1 + \frac{C_1^2}{\lambda_1} + \lambda_2 C_2^2 z_2^T z_2 + \frac{\left\|\tilde{W}_1^T\right\|^2}{\lambda_2} \\ &\le -a_1 \sum_{i=1}^{3} k_{1i} e_{1i}^{2\pi_1} - a_1 \sum_{i=1}^{3} k_{2i} e_{2i}^{2\pi_1} - \left(a_1 s_1 - \frac{1}{2} a_1{}^2\right) e_2^T e_2 \\ &\quad - \frac{1}{2} G_{m1} \tilde{a}_1{}^2 + \frac{1}{2\varepsilon^2} G_{m1} - \frac{1}{2} G_{n1} \left\|\tilde{W}_1\right\|^2 + \frac{1}{2} G_{n1} \bar{W}_1^2 \\ &\quad - \Sigma_1^T (Q_1 - \lambda_1 I - \hbar_1)\Sigma_1 + \frac{C_1^2}{\lambda_1} + \frac{\left\|\tilde{W}_1^T\right\|^2}{\lambda_2}, \end{aligned} \tag{31}$$

where

$$\hbar_1 = \begin{bmatrix} 0_{3\times3} & 0_{3\times3} \\ 0_{3\times3} & \left(\frac{1}{2} + \lambda_2 C_2^2\right) I_{3\times3} \end{bmatrix}, \tag{32}$$

and I is the identity matrix.

Define $BU = [T_{u1}, T_{u2}, T_{u3}]^T$. With the desired yaw angle ψ_d given, the corresponding attitude angles ϕ_d and θ_d and required propeller lift u_1 can be calculated as [35]

$$\begin{aligned} \phi_d &= \arctan \frac{\cos\theta_d (T_{u1} \sin\psi_d - T_{u2} \cos\psi_d)}{T_{u3}}, \\ \theta_d &= \arctan \frac{T_{u1} \cos\psi_d + T_{u2} \sin\psi_d}{T_{u3}}, \\ u_1 &= \frac{m T_{u3}}{\cos\theta_d \cos\varphi_d}. \end{aligned} \tag{33}$$

3.3. VGESO Design of Attitude Motion. Similarly, the attitude equation of the quadrotor UAV can be rewritten as

$$\begin{aligned} \dot{\Xi} &= H\aleph, \\ \dot{\aleph} &= -J^{-1}\aleph \times J\aleph + \rho_2 J^{-1} M + d_2, \end{aligned} \tag{34}$$

where H is the attitude transition matrix and $\rho_2 = \mathrm{diag}\{\rho_{21}, \rho_{22}, \rho_{23}\}$.

Considering the unknown actuator fault ρ_2, RBFNNs are adopted to approximate the coupling term $\rho_2 J^{-1} M$, which is in the form of

$$L_2 \rho_2 J^{-1} M = W_2^{*T} h\left(J^{-1} M\right) + \wp_2^*, \tag{35}$$

where $L_2 = L_2^T > 0$ is the designed parameter, $W_2 \in R^{j\times3}$ is the optimal weight satisfying $\|W_2^*\| \le \bar{W}_2$, $h(J^{-1}M) \in R^{j\times1}$ is the Gaussian function which satisfies $\|h(J^{-1}M)\| \le \delta_2$, and $\wp_2^*$ is the approximate error.

Define $\aleph = x_3$ and $d_2 = x_4$. Then, we have

$$\begin{aligned} \dot{x}_3 &= -J^{-1} x_3 \times J x_3 + L_2^{-1} W_2^{*T} h\left(J^{-1} M\right) + L_2^{-1} \wp_2^* + x_4, \\ \dot{x}_4 &= \dot{d}_2. \end{aligned} \tag{36}$$

Based on (36), the VGESO is established as

$$\begin{aligned} \dot{\hat{x}}_3 &= -J^{-1} x_3 \times J x_3 + L_2^{-1} \hat{W}_2^T h\left(J^{-1} M\right) + \hat{x}_4 - \beta_3(t) z_3, \\ \dot{\hat{x}}_4 &= -\beta_4(t) z_3, \end{aligned} \tag{37}$$

where $\hat{x}_3$ and $\hat{x}_4$ are the estimations of x_3 and x_4; $z_3 = \hat{x}_3 - x_3$;

$$Y_2(t) = \begin{cases} \dfrac{\gamma_3}{\|z_3\|^2}, & \|z_3\| \ge h_2, \\ \gamma_4, & \text{other}; \end{cases} \tag{38}$$

$\beta_3(t) = \mathrm{diag}\{Y_2(t)/2, Y_2(t)/2, Y_2(t)/2\}$; $\beta_4(t) = \mathrm{diag}\{Y_2(t), Y_2(t), Y_2(t)\}$; $\hat{W}_2$ is the estimation of W_2; and γ_3, h_2, and γ_4 are the prepared positive constants.

Considering (36) and (37), the observation errors of the VGESO are given by

$$\begin{aligned} \dot{z}_3 &= L_2^{-1} \tilde{W}_2^T h\left(J^{-1} M\right) - L_2^{-1} \wp_2^* + z_4 - \beta_3(t) z_3, \\ \dot{z}_4 &= -\dot{d}_2 - \beta_4(t) z_3, \end{aligned} \tag{39}$$

where $z_4 = \hat{x}_4 - x_4$ and $\tilde{W}_2 = \hat{W}_2 - W_2^*$.

Let $\Sigma_2 = [z_3, z_4]^T$. Then, we can obtain

$$\begin{aligned} \dot{\Sigma}_2 &= \begin{bmatrix} \dot{z}_3 \\ \dot{z}_4 \end{bmatrix} = \begin{bmatrix} -\beta_3(t) & 1 \\ -\beta_4(t) & 0 \end{bmatrix} \Sigma_2 + \begin{bmatrix} L_2^{-1} \tilde{W}_2^T h\left(J^{-1} M\right) \\ 0 \end{bmatrix} \\ &\quad + \begin{bmatrix} -L_2^{-1} \wp_2^* \\ -\dot{d}_2 \end{bmatrix} = A_2 \Sigma_2 + B_3 + B_4. \end{aligned} \tag{40}$$

For the purpose of ensuring that A_2 is Hurwitz matrix, the parameters satisfy $\beta_3(t) > 0$ and $\beta_4(t) > 0$. To put it differently, there is a positive definite matrix

$$P_2 = \begin{bmatrix} P_{21} & P_{22} \\ P_{23} & P_{24} \end{bmatrix}, \tag{41}$$

which satisfies

$$A_2{}^T P_2 + P_2 A_2 = -Q_2, \tag{42}$$

where Q_2 is the selected positive definite matrix.

3.4. Robust Fault-Tolerant Controller Design of Attitude Motion. The tracking errors of attitude motion are defined as

$$e_3 = \Xi_d - \Xi, \tag{43}$$

$$e_4 = \aleph_d - \aleph, \tag{44}$$

where $\Xi_d = [\phi_d, \theta_d, \psi_d]^T$ and $\aleph_d$ is the virtual control law.

Combining (34) and (44), the derivative of (43) can be reformulated as

$$\dot{e}_3 = \dot{\Xi}_d - H\aleph_d + He_4. \tag{45}$$

The virtual control law $\aleph_d$ is given as

$$\aleph_d = H^{-1}\left(\dot{\Xi}_d + k_3 e_3^{2\pi_1 - 1}\right), \tag{46}$$

where $k_3 = \text{diag}\,\{k_{21}, k_{22}, k_{23}\}$ is the positive design matrix.

Substituting (46) into (45) gives

$$\dot{e}_3 = -k_3 e_3^{2\pi_1 - 1} + He_4. \tag{47}$$

Then, differentiating (44) yields

$$\dot{e}_4 = \dot{\aleph}_d + J^{-1}\aleph \times J\aleph - J^{-1}\rho_2 M - d_2. \tag{48}$$

The attitude loop finite-time controller is proposed as

$$M = \frac{J}{\rho_2}\left(\dot{\aleph}_d + J^{-1}\aleph \times J\aleph - d_2 + k_4 e_4^{2\pi_1 - 1} + H^T e_3 + s_2 e_4\right), \tag{49}$$

where s_2 is the designed positive definite matrix.

Define $a_2 = \text{diag}\,\{1/\rho_{21}, 1/\rho_{22}, 1/\rho_{23}\}$. Since $\rho_{2i} \in [\varepsilon, 1]$, it can be seen that $a_{2i} \in [1, 1/\varepsilon]$. Then, (49) becomes

$$M = J\hat{a}_2\left(\dot{\aleph}_d + J^{-1}\aleph \times J\aleph - \hat{x}_4 + k_4 e_4^{2\pi_1 - 1} + H^T e_3 + s_2 e_4\right), \tag{50}$$

where $\hat{a}_2 = \text{diag}\,\{\hat{a}_{21}, \hat{a}_{22}, \hat{a}_{23}\}$ and $\hat{a}_{2i} (i = 1, 2, 3)$ is the estimation of a_{2i}.

Substituting (50) into (48) yields

$$\begin{aligned} \dot{e}_4 &= \dot{\aleph}_d + J^{-1}\aleph \times J\aleph - \frac{\hat{a}_2}{a_2}\left(\dot{\aleph}_d + J^{-1}\aleph \times J\aleph - \hat{x}_4 + k_4 e_4^{2\pi_1 - 1}\right. \\ &\quad \left. + H^T e_3 + s_2 e_4\right) - d_2 = -k_4 e_4^{2\pi_2 - 1} - H^T e_3 + z_4 - s_2 e_4 \\ &\quad - \frac{\tilde{a}_2}{a_2}\left(\dot{\aleph}_d + J^{-1}\aleph \times J\aleph - \hat{x}_4 + k_4 e_4^{2\pi_1 - 1} + H^T e_3 + s_2 e_4\right), \end{aligned} \tag{51}$$

where $\tilde{a}_2 = \hat{a}_2 - a_2$.

Choose the Lyapunov candidate function as

$$\begin{aligned} V_2 &= \frac{1}{2} e_3^T a_2 e_3 + \frac{1}{2} e_4{}^T a_2 e_4 + \frac{1}{2r_2}\tilde{a}_2{}^2 \\ &\quad + \frac{1}{2} tr\left\{\tilde{W}_2^T T_2^{-1} \tilde{W}_2\right\} + \Sigma_2^T P_2 \Sigma_2, \end{aligned} \tag{52}$$

where $r_2 > 0$ and $T_2 = T_2^T > 0$ are the designed parameters.

Considering (47) and (51), the derivative of (52) is given by

$$\begin{aligned} \dot{V}_2 &= e_3^T a_2\left(-k_3 e_3^{2\pi_1 - 1} + He_4\right) + e_4{}^T a_2\left[-k_4 e_4^{2\pi_1 - 1} - H^T e_3 + z_4\right. \\ &\quad \left. - s_2 e_4 - \frac{\tilde{a}_2}{a_2}\left(\dot{\aleph}_d + J^{-1}\aleph \times J\aleph - \hat{x}_4 + k_4 e_4^{2\pi_1 - 1} + H^T e_3 + s_2 e_4\right)\right] \\ &\quad + \sum_{i=1}^{3} \frac{1}{r_2}\tilde{a}_{2i}\dot{\hat{a}}_{2i} + tr\left\{\tilde{W}_2^T T_2^{-1}\dot{\hat{W}}_2\right\} + \Sigma_2^T P_2 \dot{\Sigma}_2 + \dot{\Sigma}_2^T P_2 \Sigma_2 \\ &\le -e_3^T a_2 k_3 e_3^{2\pi_1 - 1} + e_3^T a_2 He_4 - e_4{}^T a_2 k_4 e_4^{2\pi_1 - 1} - e_4{}^T a_2 H^T e_3 \\ &\quad + e_4{}^T a_2 z_4 - e_4{}^T a_2 s_2 e_4 - e_4{}^T \tilde{a}_2 \Gamma_2 + \sum_{i=1}^{3} \frac{1}{r_2}\tilde{a}_{2i}\dot{\hat{a}}_{2i} \\ &\quad + tr\left\{\tilde{W}_2^T T_2^{-1}\dot{\hat{W}}_2\right\} - \Sigma_2^T Q_2 \Sigma_2 + 2\Sigma_2^T P_2 B_3 + 2\Sigma_2^T P_2 B_4, \end{aligned} \tag{53}$$

where $\Gamma_2 = \dot{\aleph}_d + J^{-1}\aleph \times J\aleph - \hat{x}_4 + k_4 e_4^{2\pi_1 - 1} + H^T e_3 + s_2 e_4$.

The parameter update law and adaptive fault observer are designed as

$$\begin{aligned} \dot{\hat{W}}_2 &= -T_2\left(2h\left(J^{-1}M\right) z_3^T P_{21} L_2^{-1} + G_{n2}\hat{W}_2\right), \\ \dot{\hat{a}}_{2i} &= \text{Proj}_{\left[1, \frac{1}{\varepsilon}\right]}\{r_2 \Gamma_{2i} e_{4i}\} - r_2 G_{m2}\hat{a}_{2i}, \end{aligned} \tag{54}$$

where G_{n2} and G_{m2} are designed positive constants, $\text{Proj}\{\cdot\}$ is the projection operator, and $\Gamma_{2i}, e_{4i} (i = 1, 2, 3)$ are the ith elements of Γ_2 and e_4.

Defining $N_4 = \sum_{i=1}^{3}(1/r_2)\tilde{a}_{2i}\dot{\hat{a}}_{2i}$, $N_5 = tr\{\tilde{W}_2^T T_2^{-1}\dot{\hat{W}}_2\}$, and $N_6 = -\Sigma_2^T Q_2 \Sigma_2 + 2\Sigma_2^T P_2 B_3 + 2\Sigma_2^T P_2 B_4$, we have

$$\begin{aligned} N_4 &= \sum_{i=1}^{3} \Gamma_{2i} e_{4i}\tilde{a}_{2i} - \sum_{i=1}^{3} G_{m2}\tilde{a}_{2i} a_{2i} - \sum_{i=1}^{3} G_{m2}\tilde{a}_{2i}{}^2 \\ &\le \sum_{i=1}^{3} \Gamma_{2i} e_{4i}\tilde{a}_{2i} - \sum_{i=1}^{3} \frac{1}{2} G_{m2}\tilde{a}_{2i}{}^2 + \frac{3}{2\varepsilon^2} G_{m2}, \end{aligned} \tag{55}$$

$$\begin{aligned}N_5 &= -tr\left\{\tilde{W}_2^T 2h\left(J^{-1}M\right)z_3^T P_{21}L_2^{-1}\right\}\\ &\quad - G_{n2}tr\left\{\tilde{W}_2^T\left(\tilde{W}_2 + W_2^*\right)\right\}\\ &\le -tr\left\{\tilde{W}_2^T 2h\left(J^{-1}M\right)z_3^T P_{21}L_2^{-1}\right\} - G_{n2}\left\|\tilde{W}_2^T\right\|^2\\ &\quad + \frac{1}{2}G_{n2}\left\|\tilde{W}_2\right\|^2 + \frac{1}{2}G_{n2}\left\|W_2^*\right\|^2\\ &\le -tr\left\{\tilde{W}_2^T 2h\left(J^{-1}M\right)z_3^T P_{21}L_2^{-1}\right\}\\ &\quad - \frac{1}{2}G_{n2}\left\|\tilde{W}_2\right\|^2 + \frac{1}{2}G_{n2}\bar{W}_2^2,\end{aligned} \tag{56}$$

$$\begin{aligned}N_6 &\le -\Sigma_2^T Q_2\Sigma_2 + 2\left\|\Sigma_2^T\right\|\left\|P_2\right\|\left\|B_4\right\|\\ &\quad + 2z_3^T P_{21}L_2^{-1}\tilde{W}_2^{*T}h\left(J^{-1}M\right)\\ &\quad + 2z_4^T P_{23}L_2^{-1}\tilde{W}_2^{*T}h\left(J^{-1}M\right)\\ &\le -\Sigma_2^T(Q_2 - \lambda_3 I)\Sigma_2 + \frac{C_3^2}{\lambda_3}\\ &\quad + 2z_3^T P_{21}L_2^{-1}\tilde{W}_2^{*T}h\left(J^{-1}M\right)\\ &\quad + \lambda_4 C_4^2 z_4^T z_4 + \frac{\left\|\tilde{W}_2^T\right\|^2}{\lambda_4},\end{aligned} \tag{57}$$

where λ_3 and λ_4 are designed positive parameters, $\|P_2\|\|B_4\| \le C_3$, and $\|P_{23}\|\|L_2^{-1}\|\|h(J^{-1}M)\| \le C_4$.

Substituting (55), (56), and (57) into (53), one has

$$\begin{aligned}\dot{V}_2 &\le -e_3^T a_2 k_3 e_3^{2\pi_1 - 1} - e_4{}^T a_2 k_4 e_4^{2\pi_1 - 1} + \frac{1}{2}e_4{}^T a_2{}^2 e_4 + \frac{1}{2}\|z_4\|^2\\ &\quad - e_4{}^T a_2 s_2 e_4 - \sum_{i=1}^{3}\frac{1}{2}G_{m2}\tilde{a}_{2i}{}^2 + \frac{3}{2\varepsilon^2}G_{m2} - \frac{1}{2}G_{n2}\left\|\tilde{W}_2\right\|^2\\ &\quad + \frac{1}{2}G_{n2}\bar{W}_2^2 - \Sigma_2^T(Q_2 - \lambda_3 I)\Sigma_2 + \frac{C_3^2}{\lambda_3} + \lambda_4 C_4^2 z_4^T z_4\\ &\quad + \frac{\left\|\tilde{W}_2^T\right\|^2}{\lambda_4} \le -\sum_{i=1}^{3}a_{2i}k_{3i}e_{3i}^{2\pi_1} - \sum_{i=1}^{3}a_{2i}k_{4i}e_{4i}^{2\pi_1}\\ &\quad - \left(a_2 s_2 - \frac{1}{2}a_2{}^2\right)e_4{}^T e_4 - \frac{1}{2}G_{m2}\sum_{i=1}^{3}\tilde{a}_{2i}{}^2 + \frac{3}{2\varepsilon^2}G_{m2}\\ &\quad - \frac{1}{2}G_{n2}\left\|\tilde{W}_2\right\|^2 + \frac{1}{2}G_{n2}\bar{W}_2^2\\ &\quad - \Sigma_2^T(Q_2 - \lambda_3 I - \hbar_2)\Sigma_2 + \frac{C_3^2}{\lambda_3} + \frac{\left\|\tilde{W}_2^T\right\|^2}{\lambda_4},\end{aligned} \tag{58}$$

where

$$\hbar_2 = \begin{bmatrix} 0_{3\times3} & 0_{3\times3}\\ 0_{3\times3} & \left(\frac{1}{2} + \lambda_4 C_4^2\right)I_{3\times3}\end{bmatrix}. \tag{59}$$

3.5. Closed-Loop Stability Analysis

Theorem 7. *For the given quadrotor UAV system (1) containing actuator faults and external disturbances, the VGE-SOs are designed as (10) and (37). By applying the proposed robust fault-tolerant tracking controllers (23) and (50), all closed-loop tracking errors are bounded and convergent in finite time.*

Proof. Select the Lyapunov function as

$$V_3 = V_1 + V_2. \tag{60}$$

Considering (31) and (58), the derivative of (60) can be expressed as

$$\begin{aligned}\dot{V}_3 &\le -a_1\sum_{i=1}^{3}k_{1i}e_{1i}^{2\pi_1} - a_1\sum_{i=1}^{3}k_{2i}e_{2i}^{2\pi_1} - \left(a_1 s_1 - \frac{1}{2}a_1{}^2\right)e_2^T e_2\\ &\quad - \frac{1}{2}G_{m1}\tilde{a}_1{}^2 + \frac{1}{2\varepsilon^2}G_{m1} - \frac{1}{2}G_{n1}\left\|\tilde{W}_1\right\|^2 + \frac{1}{2}G_{n1}\bar{W}_1^2\\ &\quad - \Sigma_1^T(Q_1 - \lambda_1 I - \hbar_1)\Sigma_1 + \frac{C_1^2}{\lambda_1} + \frac{\left\|\tilde{W}_1^T\right\|^2}{\lambda_2} - \sum_{i=1}^{3}a_{2i}k_{3i}e_{3i}^{2\pi_1}\\ &\quad - \sum_{i=1}^{3}a_{2i}k_{4i}e_{4i}^{2\pi_1} - \left(a_2 s_2 - \frac{1}{2}a_2{}^2\right)e_4{}^T e_4 - \frac{1}{2}G_{m2}\sum_{i=1}^{3}\tilde{a}_{2i}{}^2\\ &\quad + \frac{3}{2\varepsilon^2}G_{m2} - \frac{1}{2}G_{n2}\left\|\tilde{W}_2\right\|^2 + \frac{1}{2}G_{n2}\bar{W}_2^2\\ &\quad - \Sigma_2^T(Q_2 - \lambda_3 I - \hbar_2)\Sigma_2 + \frac{C_3^2}{\lambda_3} + \frac{\left\|\tilde{W}_2^T\right\|^2}{\lambda_4} \le -\Phi_1 V_a + \Phi_2\\ &\quad - a_1\sum_{i=1}^{3}k_{1i}e_{1i}^{2\pi_1} - a_1\sum_{i=1}^{3}k_{2i}e_{2i}^{2\pi_1} - \sum_{i=1}^{3}a_{2i}k_{3i}e_{3i}^{2\pi_1} - \sum_{i=1}^{3}a_{2i}k_{4i}e_{4i}^{2\pi_1},\end{aligned} \tag{61}$$

where

$$\begin{aligned}\Phi_1 &= \min\left\{\frac{\lambda_{\min}(Q_1 - \lambda_1 I - \hbar_1)}{\lambda_{\max}(P_1)}, G_{m1}r_1, \frac{G_{n1} - (2/\lambda_2)}{\lambda_{\max}\left(T_1^{-1}\right)},\right.\\ &\quad \left.\frac{\lambda_{\min}(Q_2 - \lambda_3 I - \hbar_2)}{\lambda_{\max}(P_2)}, 3G_{m2}r_2, \frac{G_{n2} - (2/\lambda_4)}{\lambda_{\max}\left(T_2^{-1}\right)}\right\}, \Phi_2\\ &\quad + \frac{1}{2}a_2{}^2 + \frac{1}{2}G_{n2}\bar{W}_2^2 + \frac{C_3^2}{\lambda_3},\\ V_a &= \frac{1}{2r_1}\tilde{a}_1{}^2 + \frac{1}{2}tr\left\{\tilde{W}_1^T T_1^{-1}\tilde{W}_1\right\} + \Sigma_1^T P_1\Sigma_1 + \frac{1}{2r_2}\tilde{a}_2{}^2\\ &\quad + \frac{1}{2}tr\left\{\tilde{W}_2^T T_2^{-1}\tilde{W}_2\right\} + \Sigma_2^T P_2\Sigma_2.\end{aligned} \tag{62}$$

By the utilization of Lemma 3, we can get

$$-a_1\sum_{i=1}^{3}k_{1i}e_{1i}^{2\pi_1} \le -a_1 k_{1m}\sum_{i=1}^{3}e_{1i}^{2\pi_1} \le -a_1\bar{k}_{1m}\left(\frac{1}{2}\sum_{i=1}^{3}e_{1i}^2\right)^{\pi_1}, \tag{63}$$

$$-a_1\sum_{i=1}^{3}k_{2i}e_{2i}^{2\pi_1} \le -a_1 k_{2m}\sum_{i=1}^{3}e_{2i}^{2\pi_1} \le -a_1\bar{k}_{2m}\left(\frac{1}{2}\sum_{i=1}^{3}e_{2i}^2\right)^{\pi_1}, \tag{64}$$

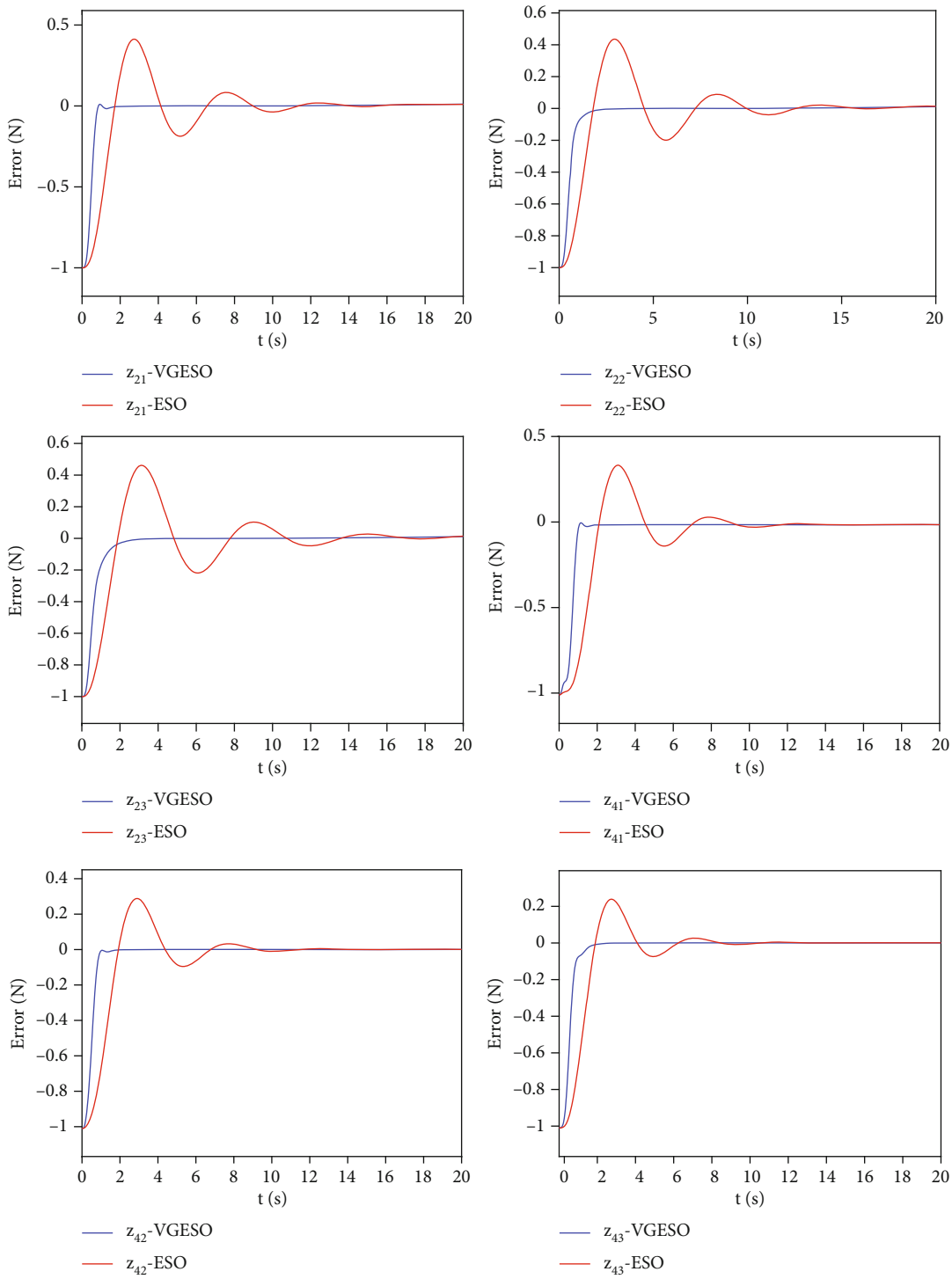

Figure 3: Observation errors of VGESO and ESO.

$$-\sum_{i=1}^{3} a_{2i}k_{3i}e_{3i}^{2\pi_1} \le -a_{2i}k_{3m}\sum_{i=1}^{3} e_{3i}^{2\pi_1} \le -a_{2i}\bar{k}_{3m}\left(\frac{1}{2}\sum_{i=1}^{3} e_{3i}^{2}\right)^{\pi_1}, \quad (65)$$

$$-\sum_{i=1}^{3} a_{2i}k_{4i}e_{4i}^{2\pi_1} \le -a_{2i}k_{4m}\sum_{i=1}^{3} e_{4i}^{2\pi_1} \le -a_{2i}\bar{k}_{4m}\left(\frac{1}{2}\sum_{i=1}^{3} e_{4i}^{2}\right)^{\pi_1}, \quad (66)$$

where $k_{1m} = \min\{k_{1i}\}$, $\bar{k}_{1m} = k_{1m}2^{\pi_1}$, $k_{2m} = \min\{k_{2i}\}$, $\bar{k}_{2m} = k_{2m}2^{\pi_1}$, $k_{3m} = \min\{k_{3i}\}$, $\bar{k}_{3m} = k_{3m}2^{\pi_1}$, $k_{4m} = \min\{k_{4i}\}$, and $\bar{k}_{4m} = k_{4m}2^{\pi_1}$.

By using Lemma 4 with $\kappa_1 = V_a$, $\kappa_2 = 1$, $\varpi_1 = \pi_1$, $\varpi_2 = 1 - \pi_1$, and $\varpi_3 = 1/\pi_1$, we can get

$$-V_a \le -V_a^{\pi_1} + (1-\pi_1)\pi_1^{\pi_1/(1-\pi_1)}. \quad (67)$$

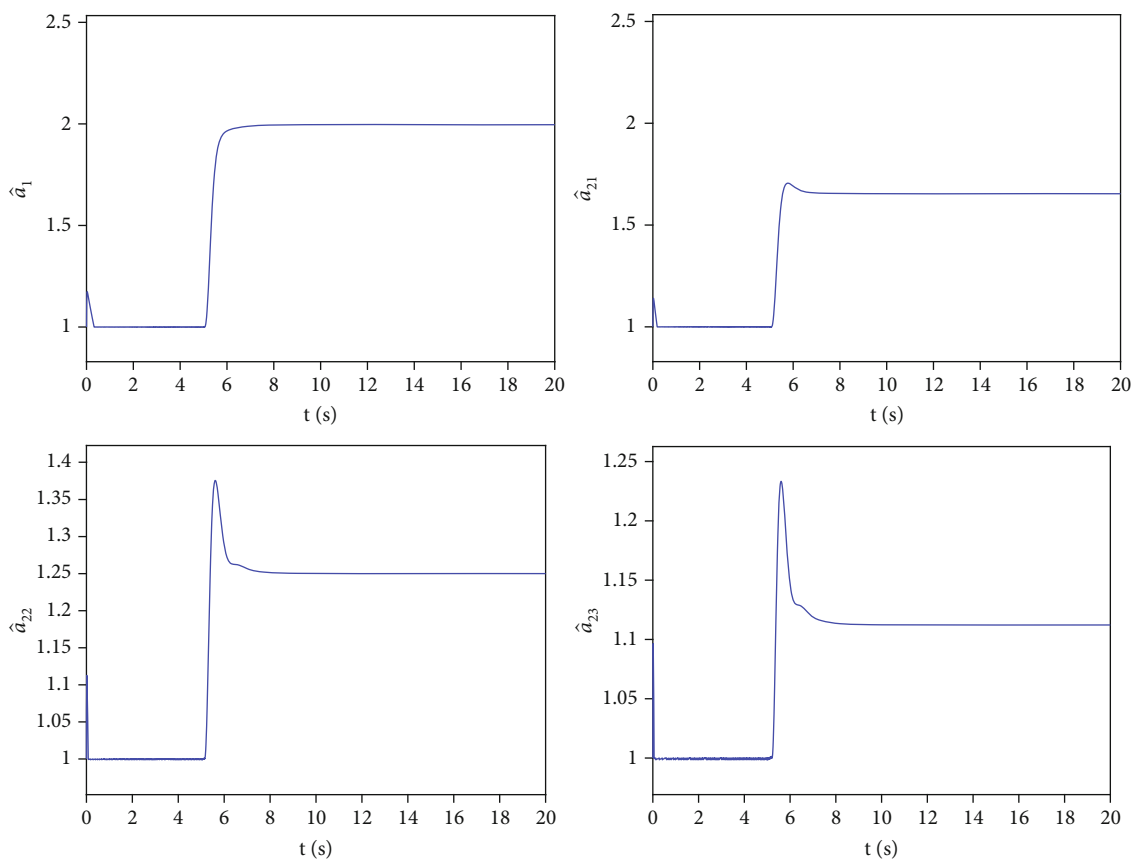

Figure 4: Actuator LOE fault factor estimations.

Combining (63), (64), (65), (66), and (67), equation (61) can be written as

$$\begin{aligned}\dot{V}_3 \le & -\Phi_1 V_a^{\pi_1} + \Phi_1(1-\pi_1)\pi_1^{\pi_1/(1-\pi_1)} + \Phi_2 - \bar{k}_{1m}\left(\frac{1}{2}a_1\sum_{i=1}^{3}e_{1i}^2\right)^{\pi_1} \\ & - \bar{k}_{2m}\left(\frac{1}{2}a_1\sum_{i=1}^{3}e_{2i}^2\right)^{\pi_1} - \bar{k}_{3m}\left(\frac{1}{2}a_{2i}\sum_{i=1}^{3}e_{3i}^2\right)^{\pi_1} \\ & - \bar{k}_{4m}\left(\frac{1}{2}a_{2i}\sum_{i=1}^{3}e_{4i}^2\right)^{\pi_1} \le -\Phi_3 V_3^{\pi_1} + \Phi_4,\end{aligned} \tag{68}$$

where $\Phi_3 = \min\{\Phi_1, \bar{k}_{1m}, \bar{k}_{2m}, \bar{k}_{3m}, \bar{k}_{4m}\}$ and $\Phi_4 = \Phi_1(1-\pi_1)\pi_1^{\pi_1/(1-\pi_1)} + \Phi_2$.

According to Lemma 5, all error signals converge in finite time. Meanwhile, the upper bound of setting time is calculated by $T_{st} \le (1/((1-\pi_1)K_d\Phi_3))[V_3^{1-\pi_1}(0) - (\Phi_4/((1-K_d)\Phi_3))^{(1-\pi_1)/\pi_1}]$ with $0 < K_d < 1$ being a constant. This concludes the above proof. □

4. Simulation Results

In this section, numerical simulations of the quadrotor UAV with actuator faults and external disturbances are carried out. The mass and inertia matrix are selected as $m = 2.1$ kg and $J = \mathrm{diag}\{0.0211, 0.0219, 0.0366\}$ Nm. The reference trajectories are chosen as $x_d = 0.5\sin(0.5t + 0.5)$ m, $y_d = 0.5\sin(0.5t)$ m, $z_d = 0.1t + 2$ m, and $\psi_d = 0.3$ rad. The parameters during the control design are chosen as $\gamma_1 = 25$, $\gamma_2 = 50$, $\gamma_3 = 25$, $\gamma_4 = 25$, $h_1 = 0.5$, $h_2 = 0.5$, $G_{n1} = 0.5$, $G_{n2} = 0.5$, $r_1 = 0.02$, $r_2 = 0.01$, $\varepsilon = 0.5$, $G_{m1} = 0.001$, $G_{m2} = 0.003$, $k_1 = \mathrm{diag}\{2, 2, 2\}$, $k_2 = \mathrm{diag}\{10, 10, 10\}$, $k_3 = \mathrm{diag}\{2, 2, 2\}$, $k_4 = \mathrm{diag}\{9, 9, 9\}$, $s_1 = \mathrm{diag}\{40, 40, 40\}$, and $s_2 = \mathrm{diag}\{20, 20, 20\}$.

To implement related numerical simulations and evaluate the observer performance, the actuator LOE fault factors are introduced

$$\begin{aligned}\rho_1 &= \begin{cases} 1, & 0 \le t < 5, \\ 0.5, & t \ge 5, \end{cases} \\ \rho_{2i} &= \begin{cases} [1, 1, 1], & 0 \le t < 5, \\ [0.6, 0.8, 0.9], & t \ge 5, \end{cases} \\ & i = 1, 2, 3.\end{aligned} \tag{69}$$

The external disturbances are assumed as

$$\begin{aligned} d_1 &= [0.1\sin(t), 0.1\sin(t), 0.1\sin(t)]^T, \\ d_2 &= [0.2\cos(t), 0.2\cos(t), 0.2\cos(t)]^T. \end{aligned} \tag{70}$$

The comparison results of the developed VGESO and traditional ESO are presented in Figure 3, where the blue

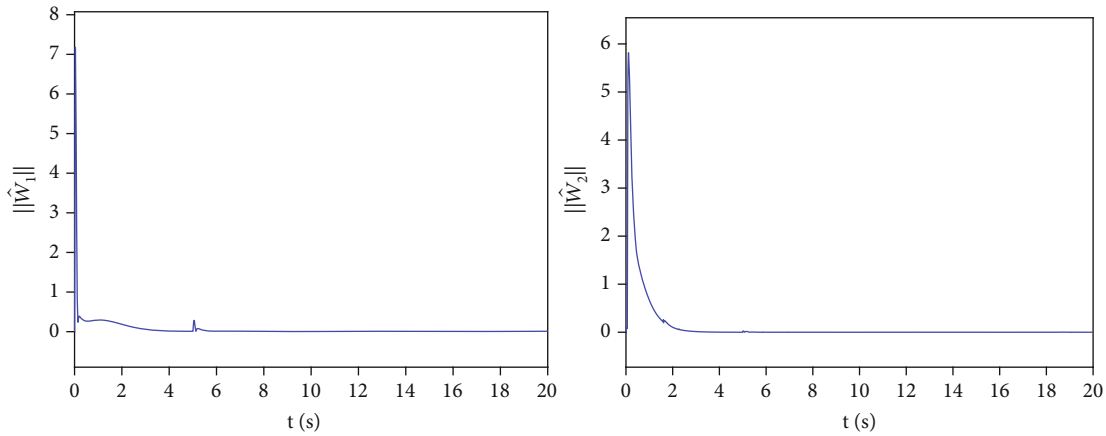

Figure 5: The norms of the optimal weight matrix.

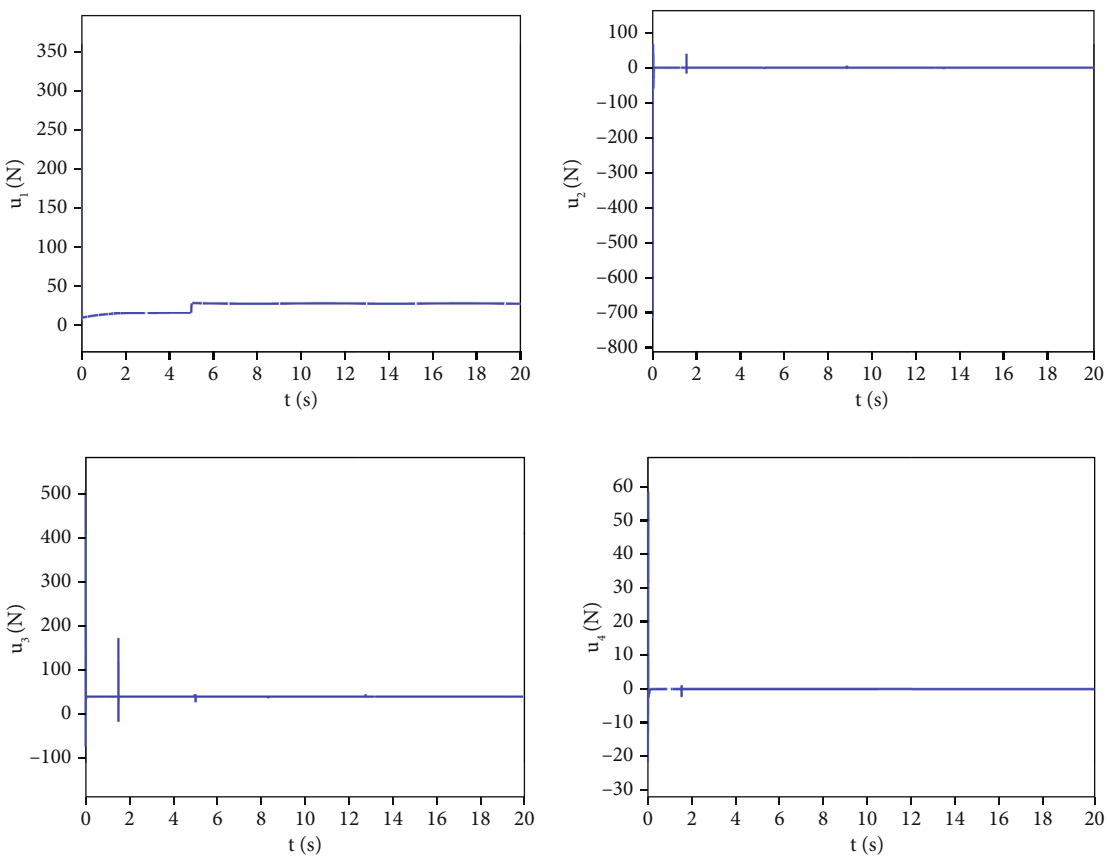

Figure 6: Actual control input signals.

lines define the observation error of VGESO and the red lines represent that of traditional ESO. From Figure 3, it can be observed that despite the traditional ESO has the ability of estimating disturbances, the so-called initial peaking phenomenon is unavoidable, which is unfavorable to the transient performance of the system. As a contrast, the developed VGESO overcomes the shortcoming by selecting a small gain at the initial phase and increasing gradually to a high value. Furthermore, to validate the feasibility of the proposed adaptive fault observer, LOE fault factors are selected as $\rho_1 = 0.5$, $\rho_{21} = 0.6$, $\rho_{22} = 0.8$, and $\rho_{23} = 0.9$. Since the output of the adaptive fault observer is the reciprocal of ρ_1 and ρ_{2i}, actual estimation values should be $\hat{a}_1 = 2$, $\hat{a}_{21} = 1.67$, $\hat{a}_{22} = 1.25$, and $\hat{a}_{23} = 1.11$. From Figure 4, it can be concluded that the adaptive fault observer can estimate the unknown actuator fault with both high accuracy and speed. Meanwhile, the norms of the NN weight matrix are displayed in Figure 5 and the corresponding control

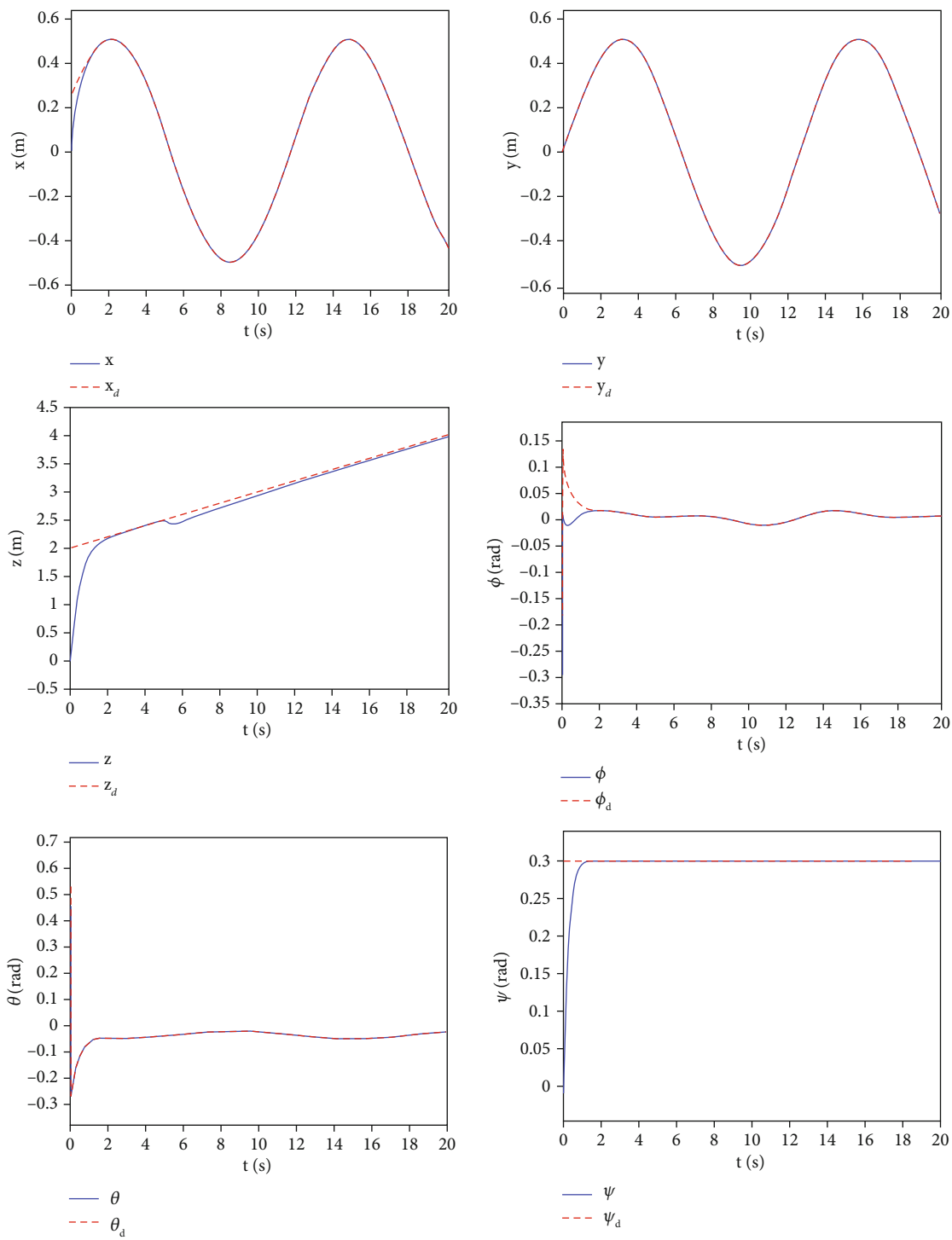

Figure 7: Tracking results with robust FTC scheme.

inputs are presented in Figure 6, respectively, which indicate that all of the simulation results are convergent and vary within reasonable limits.

The trajectory tracking results under the proposed finite-time antidisturbance FTC tactics are shown in Figure 7. From Figure 7, we can see that all states of quadrotor UAVs follow the desired trajectories, indicating the efficacy of the developed algorithm. Moreover, the comparative position tracking results under different control methods are presented in Figure 1, where trajectory A is the tracking result under the presented method, trajectory B is the tracking result under ESO-based backstepping sliding mode controller, trajectory C is the tracking result without handling the disturbance and fault, and trajectory D is the tracking result under PID controller. From Figure 8, if the negative effects derived from unknown disturbance and fault cannot be

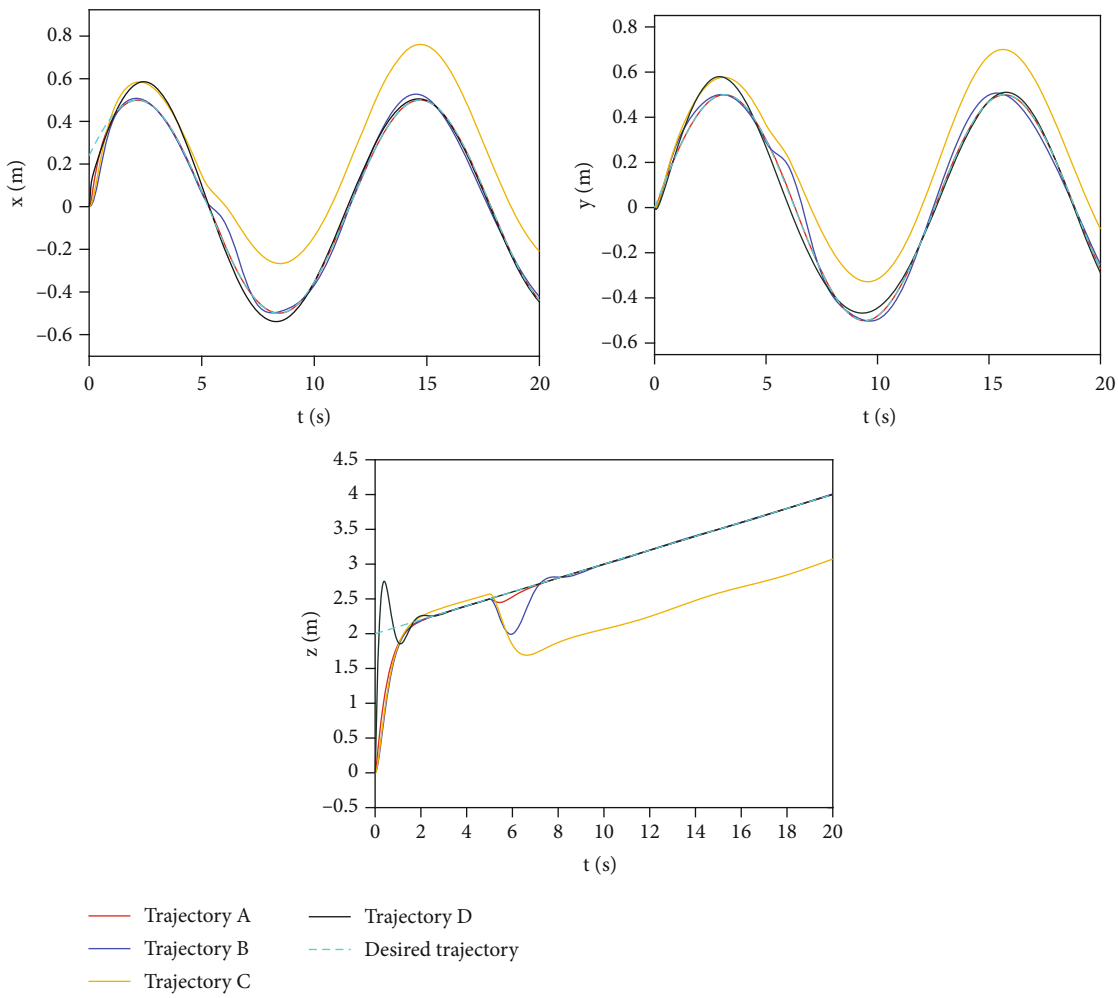

Figure 8: Position tracking results of different control methods.

eliminated in time, the desired trajectory cannot be tracked. Meanwhile, compared with the ESO-based backstepping sliding mode controller and PID controller, the given method can ensure that the quadrotor UAV has better tracking accuracy and faster convergence speed. To sum up, the developed robust adaptive finite-time FTC scheme guarantees satisfactory performance of the quadrotor UAV suffering from actuator faults and external disturbances.

5. Conclusions

In this study, a finite-time FTC strategy based on the VGESO technique has been established to solve the trajectory tracking problem of quadrotor UAV with actuator faults and unknown disturbances. Firstly, a quadrotor UAV nonlinear model has been established. Then, the VGESO has been designed to estimate unknown disturbances. Subsequently, combined with the Lyapunov stability theory, the adaptive fault observer combined with RBFNNs has been employed to estimate the fault factors. Finally, the fault-tolerant tracking controller with finite-time convergence capability has been proposed. Simulation results indicate that the developed method has superior fault tolerance and antidisturbance properties. In the future, the proposed control algorithm will be tested through quadrotor UAV flight experiments.

Data Availability

The underlying data used to support the findings of this study are available from the corresponding author upon request.

Conflicts of Interest

The authors declare that there is no conflict of interest regarding the publication of this paper.

Acknowledgments

This work was supported by the National Natural Science Foundation of China under Grants 62103315 and 52272369; the Fundamental Research Funds for the Central Universities under Grant NS2022081; the “Chunhui Plan” Cooperative Scientific Project from the Ministry of Education under Grant HZKY20220523; the Industrial Project

from the Science and Technology Department of Shaanxi Province under Grants 2022GY-243, 2023-ZDLNY-61, and 2022QFY01-16; and the Xi'an University Institutes Science and Technology Staff Service Enterprise Project under Grant 22GXFW0045.

References

[1] G. Loianno and V. Kumar, "Cooperative transportation using small quadrotors using monocular vision and inertial sensing," *Robotics and Automation Letters*, vol. 3, no. 2, pp. 680–687, 2018.

[2] G. Loianno, J. Thomas, and V. Kumar, "Cooperative localization and mapping of MAVs using RGB-D sensors," in *2015 IEEE International Conference on Robotics and Automation (ICRA)*, pp. 4021–4028, Seattle, WA, USA, 2015.

[3] J. Xiong, J. Pan, G. Chen, X. Zhang, and F. Ding, "Sliding mode dual-channel disturbance rejection attitude control for a quadrotor," *IEEE Transactions on Industrial Electronics*, vol. 69, no. 10, pp. 10489–10499, 2022.

[4] J. Theis, D. Ossmann, F. Thielecke, and H. Pfifer, "Robust autopilot design for landing a large civil aircraft in crosswind," *Control Engineering Practice.*, vol. 76, pp. 54–64, 2018.

[5] N. Sedlmair, J. Theis, and F. Thielecke, "Automatic three-point landing of a UAV with H∞ control in D-implementation," *International Federation of Automatic Control*, vol. 52, no. 12, pp. 316–321, 2019.

[6] H. Castaeda, J. Rodriguez, and G. José Luis, "Continuous and smooth differentiator based on adaptive sliding mode control for a quad-rotor MAV," *Asian Journal of Control*, vol. 23, no. 2, pp. 661–672, 2021.

[7] J. Zhang, C. Yu, and J. Ye, "Trajectory tracking control for quadrotor UAV based on extended state observer and backstepping sliding mode," *Journal of Computer Applications*, vol. 38, no. 9, p. 2742, 2018.

[8] B. Yan, P. Dai, R. Liu, M. Xing, and S. Liu, "Adaptive super-twisting sliding mode control of variable sweep morphing aircraft," *Aerospace Science and Technology*, vol. 92, pp. 198–210, 2019.

[9] S. Liu, Y. Wang, Y. Li, B. Yan, and T. Zhang, "Cooperative guidance for active defence based on line-of-sight constraint under a low-speed ratio," *The Aeronautical Journal*, vol. 127, no. 1309, pp. 491–509, 2023.

[10] B. Zhu, M. Chen, and T. Li, "Robust constrained trajectory tracking control for quadrotor unmanned aerial vehicle based on disturbance observers," *Journal of Dynamic Systems, Measurement, and Control*, vol. 142, no. 11, article 111002, 2020.

[11] D. Huang, T. Huang, N. Qin, Y. Li, and Y. Yang, "Finite-time control for a UAV system based on finite-time disturbance observer," *Aerospace Science and Technology*, vol. 129, p. 107825, 2022.

[12] H. He and H. Duan, "A multi-strategy pigeon-inspired optimization approach to active disturbance rejection control parameters tuning for vertical take-off and landing fixed-wing UAV," *Chinese Journal of Aeronautics*, vol. 35, no. 1, pp. 19–30, 2022.

[13] X. Shao, L. Wang, J. Li, and J. Liu, "High-order ESO based output feedback dynamic surface control for quadrotors under position constraints and uncertainties," *Aerospace Science and Technology*, vol. 89, pp. 288–298, 2019.

[14] Q. Zhang, Y. Fan, and C. Mao, "A gain design method for a linear extended state observers to improve robustness of deadbeat control," *IEEE Transactions on Energy Conversion*, vol. 35, no. 4, pp. 2231–2239, 2020.

[15] L. Zhao, B. Zhang, H. Yang, and Y. Wang, "Finite-time tracking control for pneumatic servo system via extended state observer," *IET Control Theory & Applications*, vol. 11, no. 16, pp. 2808–2816, 2017.

[16] J. Song, W. Shang, S. Ai, and K. Zhao, "Model and data-driven combination: a fault diagnosis and localization method for unknown fault size of quadrotor UAV actuator based on extended state observer and deep Forest," *Sensors*, vol. 22, no. 19, p. 7355, 2022.

[17] F. Chen, R. Jiang, K. Zhang, B. Jiang, and G. Tao, "Robust backstepping sliding-mode control and observer-based fault estimation for a quadrotor UAV," *IEEE Transactions on Industrial Electronics*, vol. 63, no. 8, pp. 1–5056, 2016.

[18] X. Nian, W. Chen, X. Chu, and Z. Xu, "Robust adaptive fault estimation and fault tolerant control for quadrotor attitude systems," *International Journal of Control*, vol. 93, no. 3, pp. 725–737, 2020.

[19] Y. Xiong, Y. Wu, and S. Li, "Adaptive fuzzy output feedback fault-tolerant tracking control of switched uncertain nonlinear systems with sensor faults," *Journal of the Franklin Institute*, vol. 56, no. 6, pp. 16–32, 2022.

[20] C. Guo, B. Jiang, K. Zhang, and Q. Liu, "Adaptive neural-network-based distributed fault estimation for heterogeneous multi-agent systems," *Journal of the Franklin Institute*, vol. 359, no. 16, pp. 9334–9356, 2022.

[21] M. Chen, P. Shi, and C. Lim, "Adaptive neural fault-tolerant control of a 3-DOF model helicopter system," *IEEE Transactions on Systems, Man, and Cybernetics: Systems*, vol. 46, no. 2, pp. 260–270, 2015.

[22] Y. Wang, Y. Chen, and J. Tan, "Fuzzy radial basis function neural network PID control system for a quadrotor UAV based on particle swarm optimization," in *2015 IEEE International Conference on Information and Automation*, pp. 2580–2585, Lijiang, China, 2015.

[23] S. Yang, B. Xian, and J. Cai, "Finite-time convergence control for a quadrotor unmanned aerial vehicle with a slung load," *IEEE Transactions on Industrial Informatics*, vol. 20, no. 1, pp. 605–614, 2024.

[24] B. Li, H. Ban, W. Gong, and B. Xiao, "Extended state observer-based finite-time dynamic surface control for trajectory tracking of a quadrotor unmanned aerial vehicle," *Transactions of the Institute of Measurement and Control*, vol. 42, no. 15, pp. 2956–2968, 2020.

[25] B. Li, H. Zhang, Y. Niu, D. Ran, and B. Xiao, "Finite-time disturbance observer-based trajectory tracking control for quadrotor unmanned aerial vehicle with obstacle avoidance," *Mathematical Methods in the Applied Sciences*, vol. 46, no. 1, pp. 1096–1110, 2023.

[26] W. Di, Z. Li, and D. Lv, "Adaptive finite time fault tolerant control for the quadrotor unmanned aerial vehicles based on time-triggered strategy," *Optimal Control Applications and Methods*, vol. 44, no. 1, pp. 66–80, 2023.

[27] O. Mofid and S. Mobayen, "Adaptive sliding mode control for finite-time stability of quad-rotor UAVs with parametric uncertainties," *ISA Transactions*, vol. 72, pp. 1–14, 2018.

[28] W. Xi, L. Ming, and Y. Yang, "Quadrotor flight control based on improved active disturbance rejection control technology," *Journal of Physics: Conference Series*, vol. 1948, no. 1, article 012095, 2021.

[29] K. Yan, M. Chen, Q. Wu, and B. Jiang, "Extended state observer-based sliding mode fault-tolerant control for unmanned autonomous helicopter with wind gusts," *IET Control Theory & Applications*, vol. 13, no. 10, pp. 1500–1513, 2019.

[30] H. Wang, P. Liu, and X. Zhao, "Adaptive fuzzy finite-time control of nonlinear systems with actuator faults," *IEEE Transactions on Cybernetics*, vol. 50, no. 5, pp. 1786–1797, 2020.

[31] F. Wang and X. Zhang, "Adaptive finite time control of nonlinear systems under time-varying actuator failures," *IEEE Transactions on Systems, Man, and Cybernetics-Systems*, vol. 49, no. 9, pp. 1845–1852, 2018.

[32] H. Khalil and L. Praly, "High-gain observers in nonlinear feedback control," *International Journal of Robust and Nonlinear Control*, vol. 24, no. 6, pp. 993–1015, 2014.

[33] Z. Pu, R. Yuan, J. Yi, and X. Tan, "A class of adaptive extended state observers for nonlinear disturbed systems," *IEEE Transactions on Industrial Electronics*, vol. 62, no. 9, pp. 5858–5869, 2015.

[34] J. Boskovic, L. Chen, and R. K. Mehra, "Adaptive control design for nonaffine models arising in flight control," *Journal of Guidance, Control, and Dynamics*, vol. 27, no. 2, pp. 209–217, 2004.

[35] J. Zhang, D. Gu, C. Deng, and B. Wen, "Robust and adaptive backstepping control for hexacopter UAVs," *IEEE Access*, vol. 7, pp. 163502–163514, 2019.